KSME

Springer

Journal of Mechanical Science and Technology 34 (4) 2020

Original Article
DOI 10.1007/s12206-020-0301-6

Keywords:
· Finite element
· Flutter
· Nonlinear kinematics
. Supersonic flow

Correspondence to:
Aouni A. Lakis
aouni.lakis@polymtl.ca

Citation:
Bakhtiari, M., Lakis, A. A., Kerboua, Y. (2020). Nonlinear supersonic flutter of truncated conical shells. Journal of Mechanical Science and Technology 34 (4) (2020) 1375~1388.
http://doi.org/10.1007/s12206-020-0301-6

Received April 26th, 2019
Revised January 3rd, 2020
Accepted February 4th, 2020

† Recommended by Editor
No-cheol Park

Nonlinear supersonic flutter of truncated conical shells

Mehrdad Bakhtiari, Aouni A. Lakis and Youcef Kerboua

Mechanical Engineering Department, École Polytechnique of Montréal, C.P. 6079, Succursale Centre-ville, Montréal, Québec, H3C 3A7, Canada

Abstract A numerical model was developed to investigate the flutter instability of truncated conical shells subjected to supersonic flows. The exact solution of Sanders' best first-order approximation was used to develop the finite elements model of the shell. Nonlinear kinematics of Donnell's, Sanders' and Nemeth's theories, in conjunction with the generalized coordinates method, were used to formulate the nonlinear strain energy of the shell. A pressure field was formulated using the piston theory with the correction term for the curvature. Lagrangian equations of motion based on Hamilton's principle were obtained. A variation of the harmonic balance method was used for developing the amplitude equations of the shell, and a numerical method was used for solving these equations. Results of linear and nonlinear flutter of truncated conical shells were validated against the existing data in the literature. It was observed that geometrical nonlinearities have a softening effect on the stability of the shell in supersonic flows.

1. Introduction

The aeroelastic stability of shells and plates interacting with supersonic flow has been the subject of several studies in past decades. While several studies can be found in the literature on the flutter characteristics of cylindrical shells, the number of articles on the supersonic flutter of conical shells is limited. Moreover, even in the existing studies on the flutter of cylindrical shells, very few have employed geometrically nonlinear theories in their analyses. Employing nonlinear shell theories is important since experimental studies have shown that the oscillation amplitude of flutter has the same order of magnitude as the shell thickness [1].

Dixon and Hudson [2-4] studied the flutter, vibration and buckling of truncated orthotropic thin conical shells with generalized elastic edge restraints. They employed the Donnell type of nonlinear kinematics in conjunction with the modified first-order piston theory to model the structure behavior. They argued that for shells subjected to static external pressure loads, divergence governed design conditions for small values of semi-cone angle, flutter for moderate semi-cone angle values and buckling is the dominant phenomena in large semi-cone angles. Miserentino and Dixon [5] expanded those works by performing experimental studies on the vibration and flutter of thin-walled truncated orthotropic conical shells. The experimental results provided the variations of resonant frequency with internal pressure and circumferential wave number at constant Mach number. The results verified the theoretical works of Dixon and Hudson [2] for thin shells with good accuracy. The work of Ueda et al. [6] explored the theoretical and experimental aspects of supersonic flutter in conical shells. In their experiments, they used a truncated cone with semi vertex angle of 14º to obtain flutter and buckling boundaries of the shell within supersonic flow at Mach number equal to two. They employed the finite elements method for the theoretical analysis and demonstrated good agreement between experimental and theoretical results. They also concluded that FEM is a powerful tool for predicting panel flutter behavior. Bismarck-Nasr et al. [7] developed a finite element method for supersonic flutter of truncated conical shells using Novozhilov's shell theory.

In their work on the shell model, the in-plane inertia was preserved within kinetic energy

formulations while the rotary inertia was neglected. The aerodynamic loads were modeled using the first-order high Mach number piston theory. Based on their results, it was concluded that the curvature effect in modeling the aerodynamic loads has little effect on the stability conditions.

Pidaparti [8] employed a quadrilateral thin shell finite element for analyzing the supersonic flutter of doubly curved composite shells using linear Love-Kirchhoff thin shell theory. Based on the obtained results, it was stated that the fiber angle and orthotropy impose significant effects on flutter boundaries for cylindrical and conical shells and flat plates. Sabri and Lakis [9] studied the flutter behavior of partially filled truncated conical shells in supersonic flows using a hybrid finite element method, Sanders' linear thin shell theory and first-order piston theory with correction for the effect of curvature. Initial stiffening due to pressurization was also considered in this study. Among the conclusions, it was stated that conical shells are susceptible to coupled mode flutter. Mahmoudkhani et al. [10] studied the aero-thermoelastic stability of FGM truncated conical shells in supersonic flows using Donnell's theory and the linear piston theory. They employed the eigenvalue analysis to obtain the critical parameters. They showed that larger semi-cone angles reduce the shell stability. Davar and Shokrollahi [11] provided an analysis on the supersonic flutter of FGM conical shells with clamped and simply supported boundary conditions using first-order shear deformation and linear shell theory. Their results showed that changing the boundary condition from simply supported to clamped increases all the frequencies but there is no general trend in the critical aerodynamic pressure. Vasilev [12] presented a new formulation for flutter analysis of isotropic truncated conical shells exposed to supersonic flows using linear shell theory. The author concluded that the linear piston theory significantly overestimates the critical dynamic pressure at low Mach numbers. Yang et al. [13] investigated the supersonic flutter in FGM truncated conical shells employing first-order shear deformation and linear shell theory. It was shown that it is possible to control the periodic and chaotic instabilities by varying the material's compositional profile.

As can be seen, in the earlier works other than the study of Bismarck-Nasr and Costa Savio [7], the few studies limited their kinematic models to Donnell's-type nonlinearities. Moreover, employing Galerkin approach placed additional restraints on the type of boundary conditions that can be used. The focus of the current study is to formulate a hybrid finite element model that can represent the nonlinear behavior of truncated conical shells subjected to supersonic flows using the three different shell theories of Donnell, Sanders and Nemeth. This is performed in the following steps:

- The finite element displacement functions are derived from the exact solution to Sanders' best first-order approximation.
- Using that shape function as the bases of the generalized coordinate method, the nonlinear internal strain and kinetic energies are formulated in terms of nodal degrees of freedom.

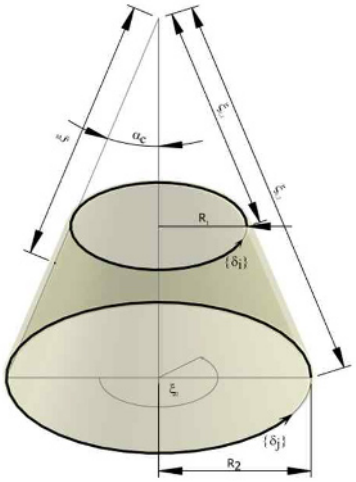

(a)

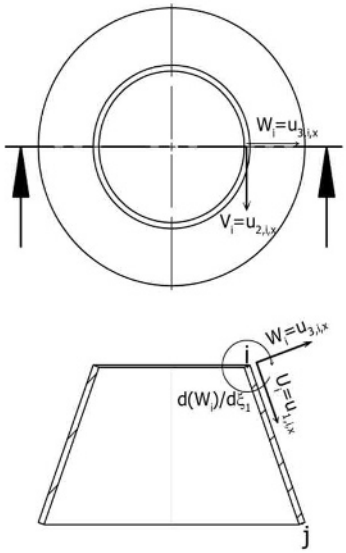

(b)

Fig. 1. Conventions: (a) Geometry and coordinate system; (b) nodal degrees of freedom.

- In addition, the effects of initial stiffening due to pressurization and axial loads are also expressed in terms of nodal displacements. Then, the Lagrangian equations of motion of the shell are developed based on the Hamilton principle.
- The equations of motion are converted to an amplitude equation by employing a variation of the harmonic balance method.

2. Nonlinear kinematics

Nemeth [14] formulated a shell theory that can provide Donnell's and Sanders' shell theories as parametric subsets [14, 15]. Fig. 1(a) shows the coordinate system and geometrical parameters of the truncated cone element of this study. The longitudinal and radial principal-curvature coordinates are de-

noted by x and θ. The cone half-angle is denoted by α_c and the slant length of the cone can be obtained from $L = x_2 - x_1$. The reference surface is assumed at the middle of the shell thickness and neglecting transverse shear deformation, there are three fundamental unknowns in this formulation: Two middle-surface tangential displacements $U = u_1(x,\theta)$ and $V = u_2(x,\theta)$ and the normal displacement $W = u_3(x,\theta)$. The displacements of material point of the shell $p(x,\theta,\xi_3)$ in the orthogonal principal-curvature coordinate systems are expressed as [16]:

$$\begin{aligned} U_1(x,\theta,\xi_3) &= u_1(x,\theta) + \xi_3\left[\varphi_1 - \varphi\varphi_2\right] \\ U_2(x,\theta,\xi_3) &= u_2(x,\theta) + \xi_3\left[\varphi_2 - \varphi\varphi_1\right] \\ U_3(x,\theta,\xi_3) &= u_3(x,\theta) - \frac{1}{2}\xi_3\left[\varphi_1^2 + \varphi_2^2\right] \end{aligned} \tag{1}$$

where ξ_3 is the normal distance from the middle surface. The linear rotation parameters φ_1, φ_2 and φ are defined as follows:

$$\begin{aligned} \varphi_1(x,\theta) &= -\frac{\partial u_3(x,\theta)}{\partial x} \\ \varphi_2(x,\theta) &= \frac{c_3 u_2(x,\theta)}{x\tan(\alpha_c)} - \frac{1}{x\sin(\alpha_c)}\frac{\partial u_3(x,\theta)}{\partial\theta} \\ \varphi(x,\theta) &= \frac{1}{2}c_3\left(\frac{\partial u_2(x,\theta)}{\partial x} - \frac{1}{x\sin(\alpha_c)}\frac{\partial u_1(x,\theta)}{\partial\theta} + \frac{u_2(x,\theta)}{x}\right) \end{aligned} \tag{2}$$

The in-plane linear deformation parameters are given as:

$$\begin{aligned} e_{11}^{\circ}(x,\theta) &= \frac{\partial u_1(x,\theta)}{\partial x} \\ e_{22}^{\circ}(x,\theta) &= \frac{1}{x\sin(\alpha_c)}\frac{\partial u_2(x,\theta)}{\partial\theta} + \frac{u_1(x,\theta)}{x} + \frac{u_3(x,\theta)}{x\tan(\alpha_c)} \\ 2e_{12}^{\circ}(x,\theta) &= \frac{1}{x\sin(\alpha_c)}\frac{\partial u_1(x,\theta)}{\partial\theta} + \frac{\partial u_2(u,\theta)}{\partial x} - \frac{u_2(x,\theta)}{x} \end{aligned} \tag{3}$$

Finally, the relationships of the strain (ε) and the linear rotation parameters (χ) with the displacements on the middle surface are expressed as follows:

$$\begin{aligned} \left\{\epsilon^{\circ}\right\} &= \begin{Bmatrix} \epsilon_{11}^{\circ} \\ \epsilon_{22}^{\circ} \\ \gamma_{12}^{\circ} \end{Bmatrix} \\ &= \begin{Bmatrix} e_{11}^{\circ} \\ e_{22}^{\circ} \\ 2e_{12}^{\circ} \end{Bmatrix} + c_{NL}\begin{Bmatrix} \frac{1}{2}\left(\varphi_1^2 + c_2\varphi^2\right) + \frac{1}{2}c_1\left[\left(e_{11}^{\circ}\right)^2 + e_{12}^{\circ}\left(e_{12}^{\circ} + 2\varphi\right)\right] \\ \frac{1}{2}\left(\varphi_2^2 + c_2\varphi^2\right) + \frac{1}{2}c_1\left[\left(e_{22}^{\circ}\right)^2 + e_{12}^{\circ}\left(e_{12}^{\circ} - 2\varphi\right)\right] \\ \varphi_1\varphi_2 + c_1\left[e_{11}^{\circ}\left(e_{12}^{\circ} - \varphi\right) + e_{22}^{\circ}\left(e_{12}^{\circ} + \varphi\right)\right] \end{Bmatrix} \end{aligned} \tag{4a}$$

$$\left\{\chi^{\circ}\right\} = \begin{Bmatrix} \chi_{11}^{\circ} \\ \chi_{22}^{\circ} \\ 2\chi_{12}^{\circ} \end{Bmatrix} = \begin{Bmatrix} \frac{\partial\phi_1}{\partial x} \\ \frac{1}{x\sin(\alpha_c)}\frac{\partial\phi_2}{\partial\theta} + \frac{\phi_1}{x} \\ \frac{1}{x\sin(\alpha_c)}\frac{\partial\phi_1}{\partial\theta} + \frac{\partial\phi_2}{x} - \frac{\phi_2}{x} + \frac{\phi}{x\tan(\alpha_c)} \end{Bmatrix} \tag{4b}$$

In the above formulation:

- Specifying $c_{NL} = 0$ and $c_3 = 1$ simplifies the kinematics to the improved first-approximation linear shell theory of Sanders [17].
- Specifying $c_{NL} = 1$ and $c_1 = c_2 = c_3 = 1$ defines Nemeth's nonlinear theory [14].
- Specifying $c_{NL} = 1$, $c_1 = 0$ and $c_2 = c_3 = 1$ retrieves Sanders' kinematics [18, 19].
- Specifying $c_{NL} = 1$, $c_1 = c_2 = 0$ and $c_3 = 1$ retrieves Sanders' kinematics with the nonlinear rotations about the normal to reference-surface are neglected [18, 19].
- Specifying $c_{NL} = 1$ and $c_1 = c_2 = c_3 = 0$ defines Donnell's strain-displacement relationship [20].

3. Constitutive equations

Using the principle of virtual work, the equilibrium equations of the shell as a function of work-conjugate stress resultants are derived based on Sanders' improved first-order linear theory [17] and given in Appendix A. Work-conjugate stress resultants of Eq. (A.2) are approximated symmetric stress-resultants and can be expressed in terms of fundamental unknowns (u_1,u_2,u_3). Hence, the two dimensional constitutive equations of the shell can be expressed as:

$$\begin{aligned} \begin{bmatrix} \{\mathrm{n}\} \\ \{\mathrm{m}\} \end{bmatrix} &= \left[CC^{\circ}\right]\left\{\mathfrak{T}^{\circ}\right\} \\ &\triangleq \left[\int_{-\frac{h}{2}}^{+\frac{h}{2}}\left(1+\frac{\xi_3}{R_1}\right)^{-1}\left(1+\frac{\xi_3}{R_2}\right)^{-1}[S]^T\left[\bar{Q}\right][S]d\xi_3\right]\left\{\mathfrak{T}^{\circ}\right\} \end{aligned} \tag{5}$$

where $\left[\bar{Q}\right]$ is the conventional plane-stress compliance tensor of the shell's material.

$$\left\{\mathfrak{T}^{\circ}\right\} = \left\{\left\{\epsilon^{\circ}\right\}^T\left\{\chi^{\circ}\right\}^T\right\}^T \tag{6}$$

Details of stress resultants of Eq. (5) and the associated constitutive matrix can be found in Appendix B of Ref. [16]. It should be noted that to produce homogeneous equilibrium equations for conical shells, the shell is approximated with a linearly variable thickness equivalent truncated cone. For such a case $\left[CC^{\circ}\right]$ shows dependency to x and the material and geometrical parameters of the shell. The constitutive matrix with substituted conical principle and geodesic radii of curvature for linearly variable thickness truncated cones is called

$\left[\overline{CC}^{\circ}\right]$ and are given in Appendix H of Ref. [16].

4. Linear solution and finite element formulation

To employ the separation of variables, homogeneous equations are required and therefore it was assumed that the thickness of the shell varies linearly along the x coordinates in a way that the actual constant thickness of the shell occurs in the middle of the element at $x_m = 0.5(x_1 + x_2)$. The displacements on the middle surface are chosen to take the following form:

$$u_1 = u_{1,\bar{x}}(\bar{x})(\cos(n_c\theta))$$
$$u_2 = u_{2,\bar{x}}(\bar{x})(\sin(n_c\theta))$$
$$u_3 = u_{3,\bar{x}}(\bar{x})(\cos(n_c\theta)) \quad (7)$$

n_c denotes the circumferential mode number and $\bar{x} = x / x_m$ is the non-dimensional longitudinal coordinates. The longitudinal part of the solution is:

$$u_{d,\bar{x}} = C_d(\bar{x})^{\frac{(\lambda-1)}{2}} \quad (8)$$

And C_d (d = 1, 2, 3) is the arbitrary magnitude of the displacement. Substituting Eq. (5) into Eq. (A.2) of Appendix A yields a system of linear differential equations that, by some lengthy mathematical manipulations, produces three equations in the following form:

$$\mathfrak{L}_{i,1}\sin(n_c\theta) + \mathfrak{L}_{i,2}\cos(n_c\theta) = 0 \ (i = 1,2,3) \quad (9)$$

$\mathfrak{L}_{i,1}$ and $\mathfrak{L}_{i,2}$ operators are solely dependent on displacements and their derivatives along x direction on the middle surface, circumferential mode number and shell parameters such as elasticity and geometry. Therefore, the only variable that shows up in $\mathfrak{L}_{i,1}$ is λ. Hence, the equilibrium Eq. (8) can be rewritten in the following matrix form:

$$[\mathcal{AQ}]\{A\} = \begin{bmatrix} \mathcal{AQ}_{1,1} & \mathcal{AQ}_{1,2} & \mathcal{AQ}_{1,3} \\ \mathcal{AQ}_{2,1} & \mathcal{AQ}_{2,2} & \mathcal{AQ}_{2,3} \\ \mathcal{AQ}_{3,1} & \mathcal{AQ}_{3,2} & \mathcal{AQ}_{3,3} \end{bmatrix} \begin{Bmatrix} C_1 \\ C_2 \\ C_3 \end{Bmatrix} = 0 \quad (10)$$

Elements of $[\mathcal{AQ}]$ are polynomials in terms of λ and details of them are given in Ref. [16]. The equilibrium equations should be able to handle any arbitrary magnitude of displacement, therefore the determinant of $[\mathcal{AQ}]$ should be equal to zero. This produces a characteristic polynomial that can be solved to obtain values of λ. Solving the characteristic polynomial yields K distinct roots and the final solution of the system is obtained by summation of all these solutions:

$$u_d(x,\theta) = \left(\sum_{k=1}^{K} C_{d,k}\left(\bar{x}^{\frac{(\lambda_k-1)}{2}}\right)\right)(\sin(n_c\theta)^{se_d})(\cos(n_c\theta)^{ce_d}) \quad (11)$$

where $se_d, ce_d = 0,1$ for $d = 1,3$ and $se_d, ce_d = 1,0$ for $d = 2$. The finite element of the current study has two nodal lines and the degrees of freedom of those nodes δ_i and δ_j are shown in Fig. 1(a). For the case of isotropic materials, four degrees of freedom at each node are chosen and are shown for δ_i node in Fig. 1(b). The mathematical expression of these degrees of freedom for δ_i node is:

$$\{\boldsymbol{\delta}_m\} = \begin{Bmatrix} \delta_{i,1} \\ \delta_{i,2} \\ \delta_{i,3} \\ \delta_{i,4} \end{Bmatrix} = \begin{Bmatrix} U_x \\ V_x \\ W_x \\ \partial W_x / \partial x \end{Bmatrix} = \begin{Bmatrix} u_{1,\bar{x}}(\bar{x}_i) \\ u_{2,\bar{x}}(\bar{x}_i) \\ u_{3,\bar{x}}(\bar{x}_i) \\ \partial u_{1,\bar{x}}(\bar{x}_i) / \partial x \end{Bmatrix} \quad (12)$$

Employing Eq. (10) and recalling the linear dependency (determinant of matrix assumed to be zero) and lengthy mathematical manipulations, three unknown amplitudes of vibration (C_1, C_2, and C_3) in the displacements of Eq. (8) can be defined in terms of each element's degrees of freedom:

$$\{\boldsymbol{\delta}\}^e = \begin{Bmatrix} \{\delta_i\} \\ \{\delta_j\} \end{Bmatrix} = \begin{Bmatrix} \delta_1 \\ \delta_2 \\ \vdots \\ \delta_k \end{Bmatrix} = \begin{bmatrix} a_{1,1} & \cdots & a_{1,K} \\ \vdots & \ddots & \vdots \\ a_{K,1} & \cdots & a_{K,K} \end{bmatrix} \begin{Bmatrix} C_1 \\ \vdots \\ C_K \end{Bmatrix} = [A]\{C\} \quad (13)$$

where $[A]$ is a constant matrix. Hence:

$$\{C\} = [A]^{-1}\{\boldsymbol{\delta}\}^e \quad (14)$$

Substituting matrix form of Eq. (14) in Eq. (7) results the finite element displacement matrix:

$$\{\boldsymbol{u}\} = \begin{Bmatrix} u_1(x,\theta) \\ u_2(x,\theta) \\ u_3(x,\theta) \end{Bmatrix} = \overbrace{[R(x,\theta)][A]^{-1}}^{[N]_{3\times K}}\{\boldsymbol{\delta}\}^e \quad (15)$$

where the elements of $[R]$ follow this equation:

$$R_{d,k}(x,\theta) = \left(\frac{x}{x_m}\right)^{\frac{(\lambda_k-1)}{2}}\left(\sin(n_c\theta)^{se_d}\right)(\cos(n_c\theta)^{ce_d}) \quad (16)$$

More details on the development of this FEM solution can be found in Ref. [21].

5. Equations of motion

5.1 Overview

So far, the spatial component of the shell's motion is defined by Eq. (15). Defining $\{\delta\} = \{\delta(t)\}$ as the temporal (time-dependent) component of shell's motion, the equations of motion of the shell, can be obtained by the generalized coordinates method. Assuming the system consists of N finite ele-

ments, each with K degrees of freedom, the Lagrangian equation of motion based on Hamilton's principle can be expressed as follows:

$$\frac{d}{dt}\left[\frac{\partial T}{\partial \dot{\delta}_i}\right]-\frac{\partial T}{\partial \delta_i}+\frac{\partial V}{\partial \delta_i}+\frac{\partial V_I}{\partial \delta_i}=q_i,\ \ (i=1,2,\ldots,D) \tag{17}$$

where

- D is the total degrees of freedom of the system after assembling mass and stiffness matrices of elements and applying the constraints.
- T denotes the total kinetic energy of the system.
- V and V_I accordingly are the internal elastic strain energy and the initial stiffening strain energy due to external axial load and hydrostatic pressure of the system.
- q_i is the nodal external force.

Eq. (17) can be rewritten in matrix form as follows:

$$\frac{d}{dt}\left[\frac{\partial T}{\partial \{\dot{\delta}\}}\right]-\frac{\partial T}{\partial \{\delta\}}+\frac{\partial V}{\partial \{\delta\}}+\frac{\partial V_i}{\partial \{\delta\}}=\{q\} \tag{18}$$

5.2 Kinetic energy

Neglecting rotational and cross translational-rotational components of the kinetic energy due to absence of shear deformation in the theory of the current study and keeping the pure translational (T_T) part of the kinetic energy, the structural mass matrix for a single element can be defined as follows:

$$\left[M_T\right]^e_{K\times K}=\iint_\Omega \rho^0\left(\left[S_T\right]^T\left[S_T\right]\right)A_1A_2dxd\theta \tag{19}$$

Details of variables of Eq. (19) can be found in Ref. [16]. The structural mass matrices of all elements can be assembled to obtain the whole system mass matrix using standard finite element assembly procedures. The corresponding assembled matrix is named $\left[M_T\right]$. Finally, by performing some mathematical operations, the kinetic energy component of the equations of motion can be obtained from the following equation:

$$\frac{d}{dt}\left[\frac{\partial T}{\partial \{\dot{\delta}\}}\right]=\left[M_S\right]\{\ddot{\delta}\}\triangleq\left(2\left[M_T\right]\right)\{\ddot{\delta}\} \tag{20}$$

$\left[M_S\right]$ denotes the assembled structural mass matrix of the whole system.

5.3 Internal strain energy

The internal strain energy over the shell element surface area (Ω) is defined as:

$$V_e=\frac{1}{2}\int_\Omega\left(\int_{-h/2}^{h/2}\left\{\sigma^{\xi_3}\right\}^T\left\{\epsilon^{\xi_3}\right\}\left(1+\frac{\xi_3}{R_1}\right)\left(1+\frac{\xi_3}{R_2}\right)d\xi_3\right)d\Omega \tag{21}$$

The through-the-thickness integral of Eq. (21) can be obtained as follows:

$$\int_{-h/2}^{h/2}\left\{\sigma^{\xi_3}\right\}^T\left\{\epsilon^{\xi_3}\right\}\left(1+\frac{\xi_3}{R_1}\right)\left(1+\frac{\xi_3}{R_2}\right)d\xi_3=\left\{\mathfrak{T}^\circ\right\}^T\left[\overline{CC}^\circ\right]\left\{\mathfrak{T}^\circ\right\} \tag{22}$$

The strain vector $\left\{\mathfrak{T}^\circ\right\}$ has two linear and nonlinear components:

$$\left\{\mathfrak{T}^\circ\right\}=\left[S_{\mathfrak{T}_L^\circ}\right]_{3\times K}\{\delta\}^e_{K\times 1}+\left[S_{\mathfrak{T}_{NL}^\circ}\right]_{3\times K^2}\left\{\delta^{\otimes 2}\right\}^e_{K^2\times 1} \tag{23}$$

where $\left\{\delta^{\otimes p}\right\}$ is the Kronecker product power p of vector $\{\delta\}$ (e.g. $\left\{\delta^{\otimes 2}\right\}=\{\delta\}\otimes\{\delta\}$). The rows of $\left[S_{\mathfrak{T}_L^\circ}\right]$ and $\left[S_{\mathfrak{T}_{NL}^\circ}\right]$ are provided in Appendix I of Ref. [16]. Using Eqs. (23) and (24) the following stiffness matrices for each element can be defined:

$$\begin{aligned}
\left[K_{11}\right]^e&\triangleq\iint_\Omega\left[S_{\mathfrak{T}_L^\circ}\right]^T\left[\overline{CC}^0\right]\left[S_{\mathfrak{T}_L^\circ}\right]A_1A_2dxd\theta\\
\left[K_{21}\right]^e&=\left(\left[K_{12}^e\right]\right)^T\triangleq\iint_\Omega\left[S_{\mathfrak{T}_{NL}^\circ}\right]^T\left[\overline{CC}^0\right]\left[S_{\mathfrak{T}_L^\circ}\right]A_1A_2dxd\theta\\
\left[K_{22}\right]^e&\triangleq\iint_\Omega\left[S_{\mathfrak{T}_{NL}^\circ}\right]^T\left[\overline{CC}^0\right]\left[S_{\mathfrak{T}_{NL}^\circ}\right]A_1A_2dxd\theta
\end{aligned} \tag{24}$$

Hence, the strain energy of the element can be written in the following form:

$$\begin{aligned}
V_e=\frac{1}{2}\Big(&\left(\{\delta\}^e\right)^T\left[K_{11}\right]^e\{\delta\}^e+\left(\{\delta\}^e\right)^T\left[K_{12}\right]^e\left\{\delta^{\otimes 2}\right\}^e\\
&+\left(\left\{\delta^{\otimes 2}\right\}^e\right)^T\left[K_{21}\right]^e\{\delta\}^e+\left(\left\{\delta^{\otimes 2}\right\}^e\right)^T\left[K_{22}\right]^e\left\{\delta^{\otimes 2}\right\}^e\Big)
\end{aligned} \tag{25}$$

The total strain energy is equal to the sum of the strain energies of all elements. Therefore, using standard finite element assembly procedures, the structural stiffness matrices of all elements can be assembled into the whole system stiffness matrices. The corresponding assembled stiffness matrices are named $\left[K_{11}\right]$, $\left[K_{12}\right]$, $\left[K_{21}\right]$ and $\left[K_{22}\right]$. But substituting Eq. (25) into Eq. (18) requires proper mathematical formulation for the derivative of Kronecker powers of vectors using matrix calculus. The necessary mathematical formulations have been developed by the authors and can be found in Ref. [22] and Appendix J of Ref. [16]. Subsequently, the derivative of the strain energy with respect to the degrees of freedom can be expressed as:

$$\frac{\partial V}{\partial \{\delta\}}=\left[K_{11}\right]\{\delta\}+\left[\tilde{K}_{12}\right]\left\{\delta^{\otimes 2}\right\}+\frac{1}{2}\left[\tilde{K}_{22}\right]\left\{\delta^{\otimes 3}\right\} \tag{26}$$

where $\left[\tilde{K}_{12}\right]$ and $\left[\tilde{K}_{22}\right]$ are formulated based on $\left[K_{12}\right]$, $\left[K_{21}\right]$ and $\left[K_{22}\right]$ using matrix calculus operations with details that are provided in Ref. [22].

5.4 Aerodynamic pressure field

The improved linear piston theory that takes into account the effect of curvature, suggests the following relationship for the aerodynamic pressure field over the shell [23, 24]:

$$P_{Aero,L} = -C_{A,1}\left[C_{A,2}\dot{u}_3 + \frac{\partial u_3}{\partial x} - C_{A,3}\frac{u_3}{x\tan(\alpha_c)}\right] \tag{27}$$

where

$$C_{A,1} = \frac{\gamma_a P_l M_l^2}{\left(M_l^2-1\right)^{1/2}},\quad C_{A,2} = \frac{1}{M_l a_l}\left(\frac{M_l^2-2}{M_l^2-1}\right),$$
$$C_{A,3} = \frac{1}{2\left(M_l^2-1\right)^{1/2}} \tag{28}$$

And γ_a, P, M, and a accordingly denote the adiabatic index, static pressure, Mach number and speed of sound. The subscript l denotes the local stream condition after the conical shock at the tip of the cone that can be obtained from the free stream condition (denoted by ∞ symbol) using Taylor-Maccoll analysis or pre-calculated look-up tables. To express the aerodynamics pressure field in terms of nodal displacements, first recalling Eq. (15), the displacement along the third curvilinear coordinates is:

$$u_3 = \left[N_W\right]\left\{\delta_e\right\} = \left[0 \quad 0 \quad 1\right]\left[N\right]\left\{\delta_e\right\} \tag{29}$$

Substituting Eq. (29) in Eq. (27) yields:

$$\left\{p_{AERO}\right\} = -C_{A,1}C_{A,2}\left[N_W\right]\left\{\dot{\delta}_e\right\} - \left(C_{A,1}\frac{\partial}{\partial x}\left[N_W\right] - \frac{C_{A,1}C_{A,3}}{x\tan(\alpha_c)}\left[N_W\right]\right)\left\{\delta_e\right\} \tag{30}$$

The general nodal force vector as a result of this pressure field is defined as:

$$\left\{q_{AERO}\right\}^e = \iint_\Omega \left[N\right]^T\left\{p_{AERO}\right\}A_1A_2 dxd\theta \tag{31}$$

Hence substituting Eq. (29) into Eq. (31) yields aerodynamics stiffness and damping matrices as follows:

$$\left[K_{AERO}\right]^e = -C_{A,1}C_{A,2}\iint_\Omega \left[N\right]^T\left[N_W\right]A_1A_2 dxd\theta + C_{A,1}C_{A,3}\iint_\Omega \left[N\right]^T\frac{1}{x\tan(\alpha_c)}\left[N_W\right]A_1A_2 dxd\theta$$

$$\left[C_{AERO}\right]^e = -C_{A,1}\iint_\Omega \left[N\right]^T\frac{\partial}{\partial x}\left[N_W\right]A_1A_2 dxd\theta \tag{32}$$

The whole structure aerodynamics and stiffness matrices $\left[K_{AERO}\right]$ and $\left[C_{AERO}\right]$ can be constructed using classic finite element assembly procedures.

5.5 Initial stiffening due to axial load and hydrostatic pressure

The stress resultants due to the combination of the axial load F_A and hydrostatic pressure p_m can be formulated as follows [25]:

$$\mathfrak{n}_{\theta A} = -x\tan(\alpha_c)p_m$$
$$\mathfrak{n}_{xA} = -\frac{x\tan(\alpha_c)}{2}p_m - \frac{F_A}{\pi\sin(2\alpha_c)} \tag{33}$$

An element's strain potential energy as a result of these stress resultants is equal to [9]:

$$V_i^e = \iint_\Omega\left[\mathfrak{n}_{\theta A}\varphi_1^2 + \mathfrak{n}_{xA}\varphi_2^2\left(\mathfrak{n}_{\theta A}+\mathfrak{n}_{xA}\right)\varphi_1^2\right]A_1A_2 dxd\theta \tag{34}$$

Defining $\left[N_U\right]=\left[1\,0\,0\right]\left[N\right]$ and $\left[N_V\right]=\left[0\,1\,0\right]\left[N\right]$ and taking the same approach as Eqs. (29) and (30), the linear rotation parameters of Eq. (2) can be expressed in terms of nodal displacements:

$$\left[N_{\varphi 1}\right] = -\frac{\partial}{\partial x}\left[N_W\right]$$
$$\left[N_{\varphi 2}\right] = \frac{1}{x\tan(\alpha_c)}\left[N_V\right] - \frac{1}{x\sin(\alpha_c)}\frac{\partial}{\partial\theta}\left[N_W\right]$$
$$\left[N_\varphi\right] = \frac{1}{2}\left(\frac{\partial}{\partial x}\left[N_V\right] - \frac{1}{x\sin(\alpha_c)}\frac{\partial}{\partial\theta}\left[N_U\right] + \frac{1}{x}\left[N_V\right]\right) \tag{35}$$

Therefore, the initial stiffness matrices due to hydrostatic pressure and axial load are obtained as follows:

$$\left[K_{i,pm}\right]^e = p_m\iint_\Omega\left(-x\tan(\alpha_c)\left[N_{\varphi 1}\right]^T\left[N_{\varphi 1}\right] + \frac{x\tan(\alpha_c)}{2}\left[N_{\varphi 2}\right]^T\left[N_{\varphi 2}\right] - x\tan(\alpha_c)\left[N_\varphi\right]^T\left[N_\varphi\right]\right)A_1A_2 dxd\theta$$
$$\left[K_{i,FA}\right]^e = F_A\iint_\Omega\left(\frac{1}{\pi\sin(2\alpha_c)}\left[N_{\varphi 2}\right]^T\left[N_{\varphi 2}\right] + \frac{1}{\pi\sin(2\alpha_c)}\left[N_\varphi\right]^T\left[N_\varphi\right]\right)A_1A_2 dxd\theta \tag{36}$$

Using general finite elements assembly procedures, the whole structure initial stiffening matrices $\left[K_{i,pm}\right]$ and $\left[K_{i,FA}\right]$ can be constructed. Therefore, employing the same approach

described for the internal strain energy, the initial stiffness component of the equations of motions is:

$$\frac{\partial V_i}{\partial\{\delta\}} = \left[K_{i,pm}\right]\{\delta\} + \left[K_{i,FA}\right]\{\delta\} \tag{37}$$

5.6 Equations of motion in terms of nodal displacements

Substituting Eqs. (20), (26), (33) and (37) in Eq. (18) results in the following equation of motion:

$$\left[M_S\right]\{\ddot{\delta}\} + \left[C_{AERO}\right]\{\dot{\delta}\} + \left[K_{tot}\right]\{\delta\} + \left[\tilde{K}_{12}\right]\{\delta^{\otimes 2}\} + \frac{1}{2}\left[\tilde{K}_{22}\right]\{\delta^{\otimes 3}\} = \{q\} \tag{38}$$

where

$$\left[K_{11,tot}\right] = \left[K_{11}\right] + \left[K_{AERO}\right] + \left[K_{i,pm}\right] + \left[K_{i,FA}\right] \tag{39}$$

6. Dynamic stability in supersonic flow

6.1 Harmonic motion

In case of free motion when there is no excitation force, the left hand side of Eq. (38) should be equal to zero or a negligible residual such as R(t):

$$R(t) = \left[M_S\right]\{\ddot{\delta}\} + \left[C_{AERO}\right]\{\dot{\delta}\} + \left[K_{11,tot}\right]\{\delta\} + \left[\tilde{K}_{12}\right]\{\delta^{\otimes 2}\} + \frac{1}{2}\left[\tilde{K}_{22}\right]\{\delta^{\otimes 3}\} \tag{40}$$

A variation of the harmonic balance method proposed by Lewandowski [26] is used to obtain the nonlinear response of the system. The temporal component of the response is assumed to have the following periodical structure:

$$\{\delta\} = \{\delta_c\}\cos(\omega t) + \{\delta_s\}\sin(\omega t) \tag{41}$$

In order to obtain the amplitude equation, the in-time Galerkin method is applied to the residual [27]:

$$\begin{aligned} 2/T\int_0^{T/4} R(t)\cos(\omega t)\,dt = 0 \\ 2/T\int_0^{T/4} R(t)\sin(\omega t)\,dt = 0 \end{aligned} \tag{42}$$

Defining $\{\boldsymbol{\delta}_{cs}\} = \left\{\{\boldsymbol{\delta}_c\}\ \{\boldsymbol{\delta}_s\}\right\}^T$, substituting Eq. (41) into Eq. (40), rearranging in the matrix form and some lengthy mathematical operations yield the following amplitude equation:

$$\begin{aligned} &-\omega^2\begin{bmatrix} \frac{1}{4}M_s & \frac{1}{2\pi}M_s \\ \frac{1}{2\pi}M_s & \frac{1}{4}M_s \end{bmatrix}\{\delta_{cs}\} + \\ &\omega\begin{bmatrix} \frac{-1}{2\pi}C_{AERO} & \frac{1}{4}C_{AERO} \\ \frac{-1}{4}C_{AERO} & \frac{1}{2\pi}C_{AERO} \end{bmatrix}\{\delta_{cs}\} + \begin{bmatrix} \frac{-1}{4}K_{11,tot} & \frac{1}{2\pi}K_{11,tot} \\ \frac{-1}{2\pi}K_{11,tot} & \frac{1}{4}K_{11,tot} \end{bmatrix}\{\delta_{cs}\} \\ &+\begin{bmatrix} \frac{2}{3\pi}\tilde{K}_{12} & \frac{1}{3\pi}\tilde{K}_{12} & \frac{1}{3\pi}\tilde{K}_{12} & \frac{1}{3\pi}\tilde{K}_{12} \\ \frac{1}{3\pi}\tilde{K}_{12} & \frac{1}{3\pi}\tilde{K}_{12} & \frac{1}{3\pi}\tilde{K}_{12} & \frac{2}{3\pi}\tilde{K}_{12} \end{bmatrix}\{\delta_{cs}\}^{\otimes 2} \\ &+\begin{bmatrix} \frac{3}{16}\tilde{K}_{22} & \frac{1}{4\pi}\tilde{K}_{22} & \frac{1}{4\pi}\tilde{K}_{22} & \frac{1}{16}\tilde{K}_{22} & \frac{1}{4\pi}\tilde{K}_{22} & \frac{1}{16}\tilde{K}_{22} & \frac{1}{16}\tilde{K}_{22} & \frac{1}{4\pi}\tilde{K}_{22} \\ \frac{1}{4\pi}\tilde{K}_{22} & \frac{1}{16}\tilde{K}_{22} & \frac{1}{16}\tilde{K}_{22} & \frac{1}{4\pi}\tilde{K}_{22} & \frac{1}{16}\tilde{K}_{22} & \frac{1}{4\pi}\tilde{K}_{22} & \frac{1}{4\pi}\tilde{K}_{22} & \frac{3}{16}\tilde{K}_{22} \end{bmatrix}\{\delta_{cs}\}^{\otimes 3} = 0 \end{aligned} \tag{43}$$

where T is the period of the response.

6.2 Linear solution

Eq. (43) can be rewritten in the following compressed form where the short names for the matrices have been substituted for their expanded form:

$$\begin{aligned} &-\omega^2\left[MM_S\right]\{\delta_{cs}\} + \omega\left[CC_{AERO}\right]\{\delta_{cs}\} + \left[KK_{tot}\right]\{\delta_{cs}\} \\ &+\left[\widetilde{KK}_{12}\right]\{\delta_{cs}^{\otimes 2}\} + \left[K\tilde{K}_{22}\right]\{\delta_{cs}^{\otimes 3}\} = 0 \end{aligned} \tag{44}$$

In case of linear dynamic response, all the nonlinear terms that include Kronecker product are assumed to be zero. By factorizing $\{\delta_{cs}\}$ and dropping the trivial solution of $\{\delta_{cs}\} = 0$, Eq. (44) takes the following form:

$$-\omega^2\left[MM_S\right] + \omega\left[CC_{AERO}\right] + \left[KK_{tot}\right] = 0 \tag{45}$$

This is a classic generalized eigenvalue problem whose exact solution can be obtained using generalized Schur decomposition. In the current study, LAPACK numerical library [28] is used to solve the linear generalized eigenvalue problem and to obtain the frequencies. Linear flutter in conical and cylindrical shells is a Hopf bifurcation and occurs as a result of merging two adjacent modes; see Refs. [9, 29]. The flutter onset can be detected by appearance of negative imaginary parts in the frequencies that are obtained from the solution of the generalized eigenvalue problem. While the real parts denote the frequency, the imaginary part represents damping. Hence, a negative damping leads to instability. In the current study, an algorithm using secant method is developed to accurately identify the linear critical pressure where the flutter onset occurs. In short, using two initial guesses for dynamic pressure where one resides in the stable region and the other is placed in the unstable region, a new pressure in between is iteratively calculated using secant root-finding algorithm that yields a frequency with a very small negative imaginary part. This is a good replacement for the common trial and error that was employed in some of the earlier studies (Sabri et al. [30]; Kerboua and Lakis [31]).

6.3 Nonlinear solution

For solving the nonlinear amplitude equation a variation of

the algorithm described by Lewandowski [26] is employed. The algorithm contains two major steps. The first step utilizes trust region optimization [32] to obtain solution of generalized coordinates vector ($\{\delta_{cs}\}$) for a given constant harmonic frequency (ω). The next step utilizes the calculated vector to calculate the nonlinear components and then correct the harmonic frequency by treating it as a linear problem. The results of the linear solution or the previous amplitude step are used as the initial guess.

Let us define the following cost function:

$$F\left(\omega,\{\delta_{cs}\}\right)=-\omega^2\left[MM_S\right]\{\delta_{cs}\}+\omega\left[CC_{AERO}\right]\{\delta_{cs}\}+\left[KK_{tot}\right]\{\delta_{cs}\}+\left[\widetilde{KK}_{12}\right]\{\delta_{cs}^{\otimes 2}\}+\left[K\tilde{K}_{22}\right]\{\delta_{cs}^{\otimes 3}\} \tag{46}$$

Obviously, the solution for a desired amplitude such as A should yield $F\left(\omega,\{\delta_{cs}\}\right)=0$. But the solution also should be constrained in a way that the maximum value of the elements within $\{\delta_{cs}\}$ that are associated with displacement in normal to surface directions (W) be equal to A. Let us call such vector $\{\delta_{cs}\}_A$.

The outline of the algorithm can be described as follows:

1. In the first step of the algorithm, using a guess for ω such ω^* (the initial guess can be obtained from the linear frequencies) and keeping that constant, Eq. (46) is solved to obtain a $\{\delta_{cs}\}^*$ vector that minimizes $F\left(\omega,\{\delta_{cs}\}\right)$.
2. $\{\delta_{cs}\}^*$ vector is rescaled to $\{\delta_{cs}\}_A^*$ so it satisfies the amplitude constraint.
3. This scaled vector is substituted as a constant vector within the rearranged version of Eq. (44) that has the following form:

$$\left(-\omega^2\left[MM_S\right]+\omega\left[CC_{AERO}\right]+\left(\left[KK_{tot}\right]+\left[\widetilde{KK}_{12}\right]vecI\left(\{\delta_{cs}\}_A^*\right)+\left[K\tilde{K}_{22}\right]vecI\left(\{\delta_{cs}^{\otimes 2}\}_A^*\right)\right)\right)\{\delta_{cs}\}=0 \tag{47}$$

Mathematical definition of operator $vecI(a)$ is given in [22] but in short this operator converts the Kronecker product of two vectors into a matrix multiplication. It should be noted that since $\{\delta_{cs}\}_A^*$ is assumed constant, Eq. (47) now has the same structure as the linear generalized eigenvalue problem of Eq. (45). Solving that linear problem provides an update for ω^*.

4. The convergence is checked by calculating $F\left(\omega^*,\{\delta_{cs}\}_A^*\right)$ vector to see if the average of its absolute is below a small threshold. Otherwise, the new ω^* in addition to $\{\delta_{cs}\}_A^*$ are fed back as the initial guesses into the first step and the iteration continues until the convergence is achieved.

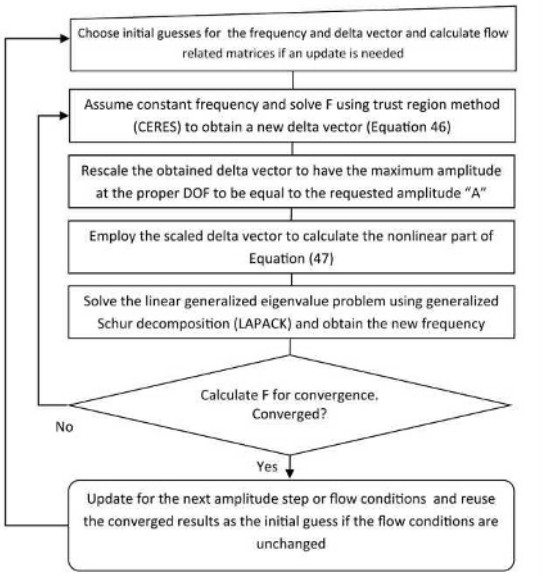

Fig. 2. Overview of the nonlinear harmonic frequency solver algorithm.

It should be noted that to ensure and improve the convergence, the implementation of the algorithm employs additional features such as concepts similar to under relaxation factor, the gradual incrementing of the amplitude and reusing the solution of the previous amplitude as the initial guess for the next larger amplitude step. The high level flowchart of the algorithm is shown in Fig. 2.

6.4 Convention of boundary conditions

Tong's [33] convention is used to identify the boundary conditions for a truncated cone that has four degrees of freedom at each end:

- F: All degrees of freedom are free (U, V, W, ∂ W/ ∂ x)].
- CC4: All degrees of freedom are clamped (U = V = W = ∂ W/ ∂ x = 0)
- SS0: Simply supported where U = 0 and the rest are free
- SS4: Simply supported where U = V = W = 0 and ∂ W/ ∂ x is free
- SS5: Where V = 0 and the rest are free

For example, F-SS0 indicates free boundary condition at the small end and simply supported according to what is described above at the larger end.

7. Results and discussion

7.1 Small amplitude vibration and flutter

It is important to validate the linear dynamic behavior of the shell to ensure the correctness of the model and also to provide a baseline for nonlinear analysis. Hence, for the first case of the current study's calculations, the small amplitude flutter of thin conical shells for the linearized version of Eq. (39) (all the nonlinear terms are dropped) was investigated by different

Table 1. Validation: Small amplitude flutter critical parameter.

Reference	Method	Λ_{cr}	n_{cr}
Shulman [34]	Galerkin, 4 terms	669	6
Dixon and Hudson [2]	Galerkin, 4 terms	492	5
	Galerkin, 8 terms	588	5
	Galerkin, 12 terms	590	5
Bismarck-Nasr and Costa Savio [7]	FEM	702	6
Sabri and Lakis [9]	Hybrid FEM	598	6
Pidaparti and Yang [36]		576	5
Mahmoudkhani et al. [10]		570	5
Present (linear)		554	5
		420	6

authors [2, 7, 9, 10, 30, 31] on a truncated conical shell with the following properties:

$t = 1.295\ \text{mm}(0.051\ \text{in})$, $R_1 = 191.72\ \text{mm}(7.548\ \text{in})$,

$L = 1558.7\ \text{mm}(61.365\ \text{in})$, $\alpha_c = 5°$,

$E = 44.82\ \text{GPa}(6.5\times10^6\ \text{lb in}^{-2})$, $\nu = 0.29$,

$\rho = 8902\ \text{kgm}^{-3}(8.33\times10^{-4}\ \text{lbf s}^2\text{in}^{-4})$, M_∞ = 3,

$a_\infty = 213\ \text{m/s}(8400\ \text{in s}^{-1})$, $\gamma = 1.4$, $P_l / P_\infty = 1.03$ and $M_l = 2.89$. M_l and P_l denote the local Mach number and pressure after the conical shock on the free stream conditions have been calculated using Ref. [35]. The boundary condition for this case is simply supported SS4. The flutter critical parameter is defined as follows:

$$\Lambda_{cr} = \frac{12\left(1-\nu^2\right)\gamma P_\infty R_1^3}{Et^3\left(M^2-1\right)^{(1/2)}} \tag{48}$$

The results including the critical circumferential mode number (n_{cr}) are shown in Table 1 and show good agreement with existing studies reported in literature. Based on the provided numbers, it seems that a few of earlier works (e.g. Refs. [9, 31]) overlooked the important effect of the formation of conical shock at the tip of the cone and subsequently the reduced local Mach number and increased local static pressure. This led to the slight differences between those values and what is reported here that practically employed the same FEM method. It seems that Schulman [34] used an insufficient number of terms in employing the Galerkin implementation. Moreover, the current study employed the correction terms for considering the effect of curvature in its linear piston theory while Dixon and Hudson [2] and Bismarck-Nasr and CostaSavio [7] ignored that effect.

The validity of real and imaginary components of the frequency of the current study were compared favorably with the work of Kerboua and Lakis [31]. The dimensions and physical properties of the shell are the same as the case presented for Table 1, $M_l = 3$ and SS4-SS4 were chosen as the local Mach number and the boundary conditions, respectively. The results

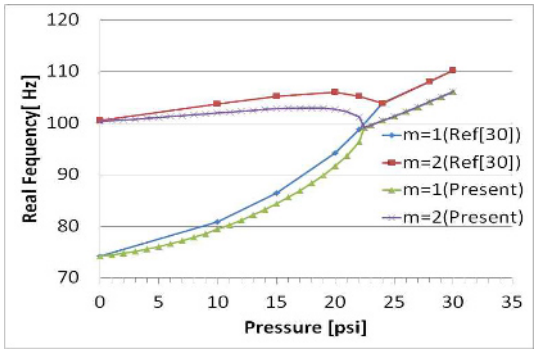

(a)

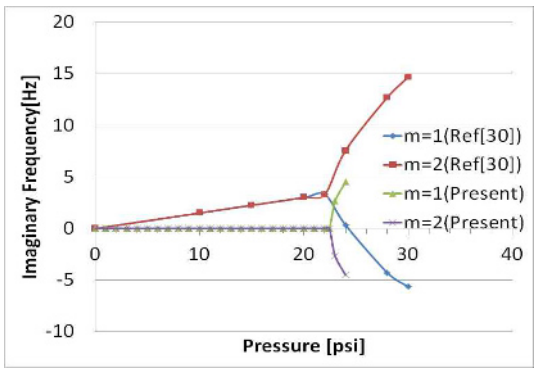

(b)

Fig. 3. Comparison of (a) the real; (b) the imaginary parts of the first and second mode of vibration with those reported by Kerboua and Lakis [31].

are shown in Fig. 3 and demonstrate good accordance. The small differences can be attributed to the Newton-Raphson iterative method that was employed for calculating the flutter onset in that study, while in the current study, the exact solution using generalized Schur decomposition is employed. In the third case, for the breathing vibration of conical shells, experimental results provided by Miserentino and Dixon [5] were selected for validation. The truncated conical shell has the following properties $t = 0.47\ \text{mm}$, $R_1 = 30.5\ \text{mm}$, $R_2 = 381\ \text{cm}$, $\alpha_c = 15°$, $E = 200\ \text{GPa}$, $\nu = 0.28$, $\rho = 7640\ \text{kgm}^{-3}$ and the boundary conditions are reported to be SS5-SS5. The shell was pressurized with air. Results for four different internal pressures are shown in Fig. 4 and demonstrate good agreement.

It should be noted that due to the configuration of the installed shell in this experiment, the internal pressure produced an axial load that was taken into account by multiplying the pressure on the sum of the shell's area at both ends. The slight difference could be attributed to the shell boundary conditions in the experiments that as described by Miserentino and Dixon [5], had some deviations from the assumed free degrees of freedom.

The flutter critical pressures and first mode frequencies at different values of internal pressure for the shell described in the second case are shown in Fig. 5. As can be seen, the flutter critical pressure increases with the internal pressure due to its

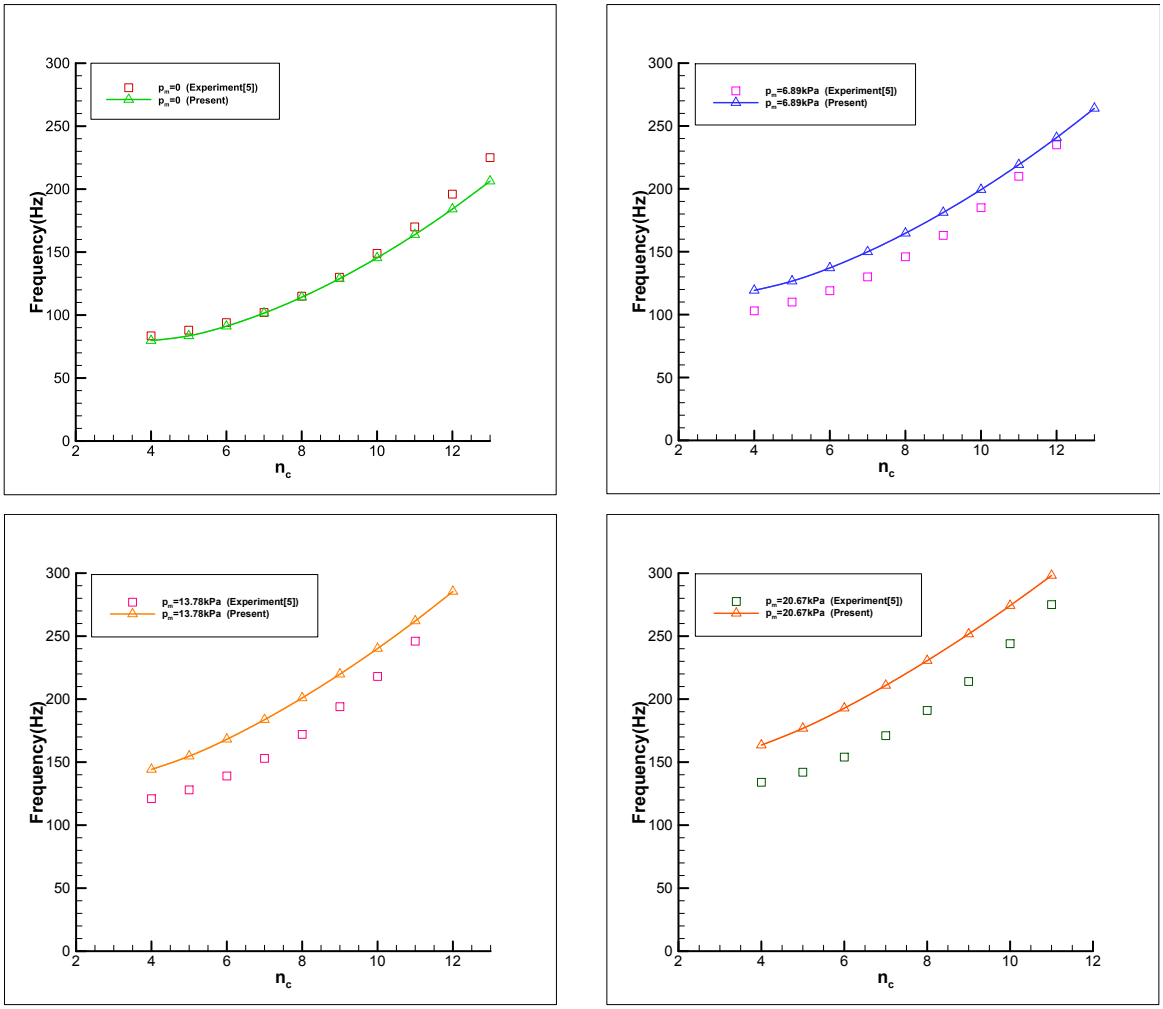

Fig. 4. Comparison of vibration frequencies of simply supported truncated conical shell at different internal pressures against those presented by Miserentino and Dixon [5].

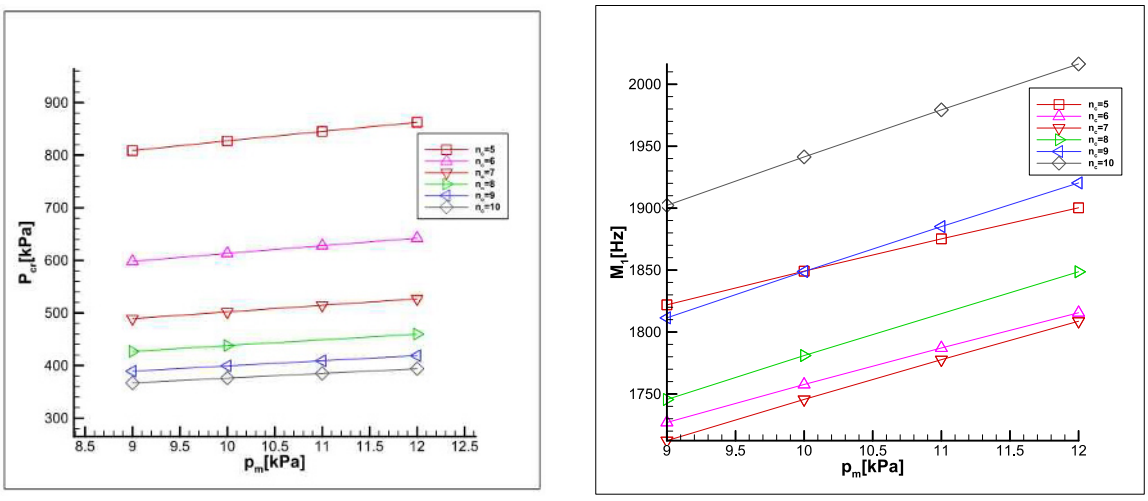

(a) (b)

Fig. 5. Pressurized shell flutter onset: (a) Critical static pressure; (b) first mode frequency for different circumferential mode numbers.

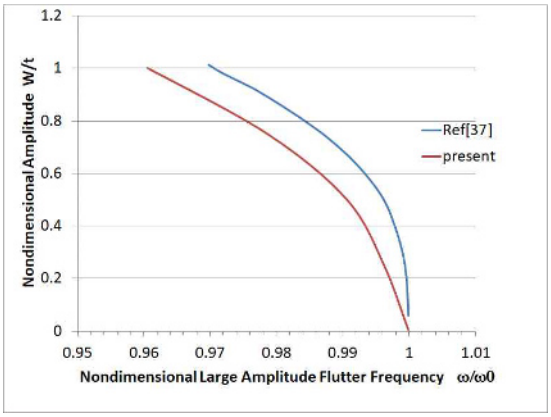

Fig. 6. Comparison of the large amplitude dimensionless flutter frequency of a cylindrical shell with Ref. [37].

stiffening effect and this is supported by what was reported by Sabri and Lakis [9] and Kerboua and Lakis [31].

7.2 Large amplitude flutter

Due to lack of enough data to reproduce the few cases of nonlinear flutter of conical shells, one case of cylindrical shell that was studied by Ref. [37] is simulated with a truncated cone with very small semi-cone angle ($\alpha_c = 0.01°$) employed for validation of large amplitude flutter. The properties are: $t = 1.016\ \text{mm}(0.004\ \text{in})$, $R_1 = 203.2\ \text{mm}(8.00\ \text{in})$, $L = 391.16\ \text{mm}$ $(15.4\ \text{in})$, $\alpha_c = 0.01°$, $E = 110.3\ \text{GPa}(16\times10^6\ \text{lbf in}^{-2})$, $\nu = 0.35$, $\rho = 8902\ \text{kgm}^{-3}(8.33\times10^{-4}\ \text{lbfs}^2\ \text{in}^{-4})$, $M_\infty = 3$, $a_\infty = 213\ \text{m/s}$ $(8400\ \text{in s}^{-1})$, $\gamma = 1.4$, $n_c = 23$ and $p_m = 3447\ \text{Pa}(0.5\ \text{psi})$. The results of large amplitude flutter static pressure to the linear flutter for different nondimensional amplitudes of vibrations are shown in Fig. 6 and demonstrate good accordance. Nonlinear flutter of a pressurized truncated cone with physical boundary conditions and geometrical properties similar to the second case was studied using Sanders' nonlinear thin shell theory for modeling the kinematics of the shell. The internal pressure was set to $p_m = 9.0\ \text{kPa}$ and the associated axial load was also considered for calculations. This is the case of a pressurized truncated conical shell that was described in the second case and was the subject of experimental study by Miserentino and Dixon [5]. The flutter critical pressure in that experiment was reported to be P_{cr} = 332.2 kPa at n_c = 9. In the current study, the linear critical pressure was calculated as Pcr = 389.305 kPa.

Investigating the first ten modes of nonlinear response that are not presented here revealed that nonlinear flutter onset and instability within the amplitude range of the current study (1.2~1.5 times of the shell thickness) occurs in the first four modes of oscillation. Hence, the presented results here are focused on those four modes. The convention in literature is to provide the stability curves in terms of static pressure. On the other hand, the common practice in the few existing experiments was to keep the static pressure constant and induce the flutter by reducing the internal pressure mostly because the gradual change in the static pressure of the supersonic wind tunnel is not practical. Hence, we focused the results around the flutter onset for varying amplitudes of vibration.

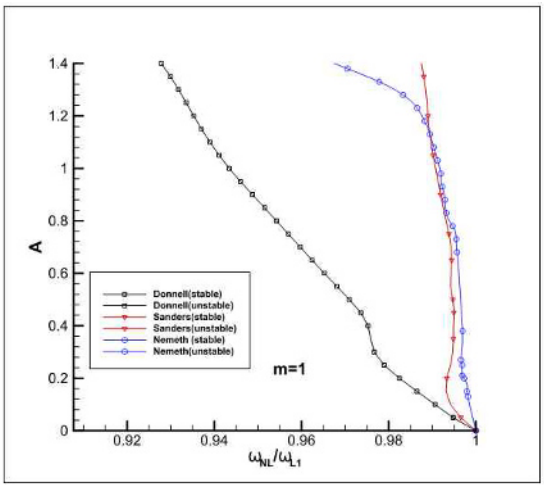

(a)

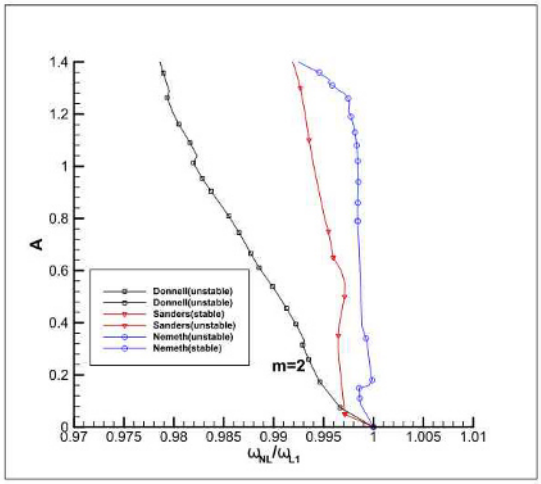

(b)

Fig. 7. Non-dimensional flutter amplitude versus non-dimensional flutter frequency; $\omega_{m,NL} / \omega_{1,L}$; (__) stable branches, (--) unstable branches; for the first and second longitudinal modes, comparison of Donnell, Sanders and Nemeth theories (n_c = 9, $\omega_{1,L}$ = 1811 Hz, P_{cr} = 389:305 kPa).

Fig. 7 shows the variation of dimensionless flutter frequency versus the amplitude of flutter vibration for all three different theories for the first and the second longitudinal modes of this case. As can be seen, all theories predicted a softening behavior for the effect of geometrical nonlinearities. Moreover, in both modes, Donnell's theory predicted a stronger softening effect but the prediction of Sanders' and Nemeth's theories at lower amplitudes are relatively close. Since the contribution of additional terms in Nemeth's theory compared to Sanders' is more effective in thicker shells and in the presence of shear deforma-

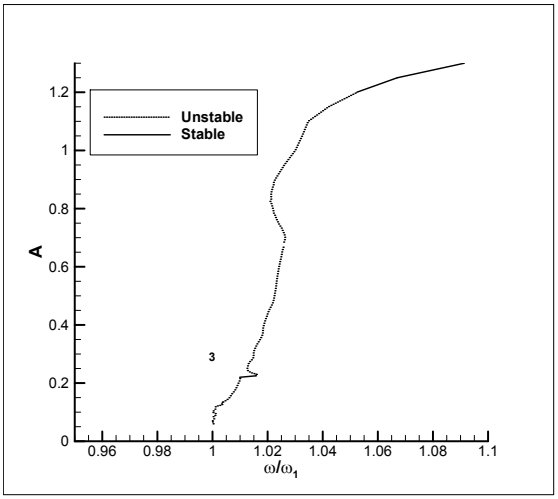

(a)

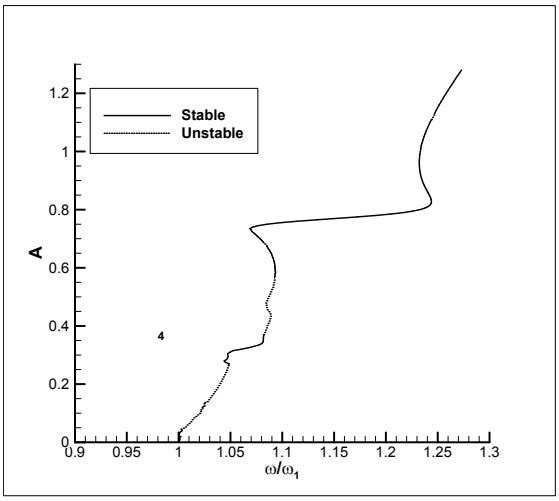

(b)

Fig. 8. Non-dimensional flutter amplitude versus non-dimensional flutter frequency; $\omega_{m,NL}/\omega_{1,L}$; (__) stable branches, (--) unstable branches; for the third and fourth longitudinal modes predicted by Sanders' nonlinear theory (n_c = 9, $\omega_{1,L}$ = 1811 Hz, P_{cr} = 389:305 kPa).

tion, producing close results for this particular thin shell is expected. Notably, all three theories predicted unstable branches of vibration for both modes that are different from toggling between stability and instability for the linear solution. This is a result of Neimark-Sacker bifurcations of the periodic orbit.

Fig. 8 shows the variation of non-dimensional flutter amplitude versus non-dimensional flutter frequency for the third and the fourth longitudinal modes of Sanders' theory. This has been calculated at a very small post-flutter critical pressure $P_{cr} = 390.0$ kPa to achieve numerical convergence.

The alternating stable-unstable behavior between modes that results in a shift in the stability to the higher modes is consistent with the general behavior described for the nonlinear flutter in cylindrical shells [29]. The next Neimark-Sacker bifurcation results in establishing the stability in lower modes while destabilizes the higher modes. Moreover, as can be seen in all of the results, the deviations from the linear frequency are not significant and that is in line with what is reported in the experimental work of Miserentino and Dixon [5]. It should be noted due to the presence of $\sin(\omega t)$ in Eq. (41), one additional mode emerges between each two linear modes. In other words, in terms of frequency, the first two modes on nonlinear vibration have close values to the first linear mode and similarly, the third and fourth nonlinear frequencies have values that emerged from the second linear mode of vibration.

8. Conclusion

A nonlinear hybrid finite element model was developed for truncated conical shells, based on the exact solution of Sander's linear shell theory. Using the generalized coordinate method and the displacement function of the FEM model, the internal strain energy of the shell for three different types of geometrical nonlinearities (Donnell, Sanders, Nemeth) was defined in terms of nodal displacement. The linear piston theory with correction term for the effect of curvature employed for modeling the pressure field and transformed in terms of nodal displacements. The effect of initial stiffening due to internal pressure and axial loads was also formulated in terms of nodal displacements. Equations of motion of the shell were developed using Lagrangian approach. Then, employing a variation of harmonic balance method, the amplitude equations of the shell were obtained. The linear flutter problem was solved using the exact solution of generalized Schur decomposition of the system and an iterative method was developed for the nonlinear solution. Results of vibration of pressurized truncated conical shells were compared with those existing in the literature, and these showed good agreement.

Linear and large amplitude flutter characteristics were also compared with the existing experimental data for conical and cylindrical shells accordingly, and these demonstrated good accordance.

The large amplitude flutter responses of truncated conical shells were obtained and these showed softening behavior. In addition, it was observed that, as the amplitude of the vibration increased, the instability shifted to higher modes due to Neimark-Sacker bifurcation.

Nomenclature

$[\mathcal{AQ}]$	: Characteristic polynomial matrix
c_{NL}, c_1, c_2, c_3	: Flag parameters to define different shell theories
$\left[\overline{CC}^{\circ}\right]$	: Symmetric constitutive matrix for conical element
e°_{11}, e°_{12}, e°_{22}	: Linear deformation parameters defined by Eq. (3)
M_{∞}, M_l	: Free stream Mach number and local flow Mach number (after the conical shock)
$[N]$	: Displacement field matrix of a finite element defined by Eq. (15)
n_c	: Circumferential mode number

References

[1] M. Amabili and F. Pellicano, Nonlinear supersonic flutter of circular cylindrical shells, *AIAA Journal*, 39 (4) (2001) 564-573.

[2] S. C. Dixon and M. L. Hudson, *Flutter, Vibration, and Buckling of Truncated Orthotropic Conical Shells with Generalized Elastic Edge Restraint,* Tech. Rep. NASA-TN-D-5759, L-6663 (1970).

[3] S. C. Dixon and M. L. Hudson, *Flutter, Vibration, and Buckling of Truncated Orthotropic Conical Shells with Generalized Elastic Edge Restraint, Supplement*, Tech. Rep. NASA-TN-D-5759-SUPPL (1970).

[4] S. C. Dixon and M. L. Hudson, *Supersonic Asymmetric Flutter and Divergence of Truncated Conical Shells with Ring Supported Edges*, Tech. Rep. NASA-TN-D-6223, L-7527 (1971).

[5] R. Miserentino and S. C. Dixon, *Vibration and Flutter Tests of a Pressurized Thin-walled Truncated Conical Shell*, Tech. Rep. NASA-TN-D-6106, L-7345 (1971).

[6] T. Ueda, S. Kobayashi and M. Kihira, Supersonic flutter of truncated conical shells, *Transactions of the Japan Society for Aeronautical and Space Sciences*, 20 (47) (1977) 13-30.

[7] M. N. Bismarck-Nasr and H. R. Costa Savio, Finite-element solution of the supersonic flutter of conical shells, *AIAA Journal*, 17 (10) (1979) 1148-1150.

[8] R. Pidaparti, Flutter analysis of cantilevered curved composite panels, *Proceedings of the 7th International Conference on Composite Structures*, 25 (1-4) (1993) 89-93.

[9] F. Sabri and A. A. Lakis, Hybrid finite element method applied to supersonic flutter of an empty or partially liquid-filled truncated conical shell, *Journal of Sound and Vibration*, 329 (3) (2010) 302-316.

[10] S. Mahmoudkhani, H. Haddadpour and H. Navazi, Supersonic flutter prediction of functionally graded conical shells, *Composite Structures*, 92 (2) (2010) 377-386.

[11] A. Davar and H. Shokrollahi, Flutter of functionally graded open conical shell panels subjected to supersonic air flow, *Proceedings of the Institution of Mechanical Engineers, Part G: Journal of Aerospace Engineering* (2012) 1036-1052.

[12] A. Vasilev, Flutter of conical shells under external flow of a supersonic gas, *Moscow University Mechanics Bulletin*, 70 (2) (2015) 23-27.

[13] S. W. Yang, Y. X. Hao, W. Zhang and S. B. Li, Nonlinear dynamic behavior of functionally graded truncated conical shell uder complex loads, *International Journal of Bifurcation and Chaos*, 25 (2) (2015) 1550025.

[14] M. P. Nemeth, *A Leonard-Sanders-Budiansky-Koiter-type Nonlinear Shell Theory with a Hierarchy of Transverse-shearing Deformations*, Tech. Rep. NASA/TP-2013-218025 (2013).

[15] M. P. Nemeth, *An exposition on the Nonlinear Kinematics of Shells, Including Transverse Shearing Deformations*, Tech. Rep. NASA/TM-2013-217964, NASA (2013).

[16] M. Bakhtiari, A. A. Lakis and Y. Kerboua, *Nonlinear Vibration of Truncated Conical Shells: Donnell, Sanders and Nemeth theories*, Tech. Rep. EPM-RT-2018-01 (2018).

[17] J. L. Sanders Jr, *An Improved First-approximation Theory for Thin Shells*, Tech. Rep. TR R-24, NASA (1959).

[18] J. L. Sanders Jr, *Nonlinear Theories for Thin Shells*, Tech. Rep. AD0253822, DTIC Document (1961).

[19] J. L. Sanders Jr, Nonlinear theories for thin shells, *Quarterly of Applied Mathematics* (1963) 21-36.

[20] L. H. Donnell, A new theory for the buckling of thin cylinders under axial compression and bending, *Trans Asme*, 56 (11) (1934) 795-806.

[21] M. Bakhtiari, A. A. Lakis and Y. Kerboua, Nonlinear vibration of truncated conical shells: Donnell, Sanders and Nemeth theories, *International Journal of Nonlinear Sciences and Numerical Simulation* (2019).

[22] M. Bakhtiari, A. A. Lakis and Y. Kerboua, Derivatives of fourth order Kronecker power systems with applications in nonlinear elasticity, *Applied Mathematics and Computation,* 362 (2019) 124501.

[23] M. Amabili, *Nonlinear Vibrations and Stability of Shells and Plates*, Cambridge University Press (2008).

[24] H. Krumhaar, *The Accuracy of Applying Linear Piston Theory to Cylindrical Shells*, Tech. Rep. AD0408387 (1963).

[25] S. G. P. Castro, C. Mittelstedt, F. A. C. Monteiro, M. A. Arbelo, R. Degenhardt and G. Ziegmann, A semi-analytical approach for linear and non-linear analysis of unstiffened laminated composite cylinders and cones under axial, torsion and pressure loads, *Thin-Walled Structures*, 90 (2015) 61-73.

[26] R. Lewandowski, Free vibration of structures with cubic non-linearity-remarks on amplitude equation and Rayleigh quotient, *Computer Methods in Applied Mechanics and Engineering,* 192 (13) (2003) 1681-1709.

[27] R. Lewandowski, Non-linear steady state vibrations of beams excited by vortex shedding, *Journal of Sound and Vibration*, 252 (4) (2002) 675-696.

[28] E. Anderson, Z. Bai, C. Bischof, L. S. Blackford, J. Demmel, J. Dongarra, J. Du Croz, A. Greenbaum, S. Hammarling and A. McKenney, *LAPACK Users' Guide,* SIAM (1999).

[29] M. Amabili and F. Pellicano, Multimode approach to nonlinear supersonic flutter of imperfect circular cylindrical shells, *Journal of Applied Mechanics*, 69 (2) (2001) 117-129.

[30] F. Sabri, A. Lakis and M. Toorani, Hybrid finite element method in supersonic flutter analysis of circular cylindrical shells, *31st International Conference on Boundary Elements and Other Mesh Reduction Methods, BEM/MRM 31*, *WIT Transactions on Modelling and Simulation,* WIT Press, 49 (2009) 233-244, ISBN 1743355X.

[31] Y. Kerboua and A. A. Lakis, Numerical model to analyze the aerodynamic behavior of a combined conical-cylindrical shell, *Aerospace Science and Technology*, 58 (2016) 601-617.

[32] S. Agarwal and K. Mierle and Others, *Ceres Solver*, http://ceres-solver.org (2018).

[33] L. Tong, Free vibration of orthotropic conical shells, *International Journal of Engineering Science*, 31 (5) (1993) 719-733.

[34] Y. Shulman, *Vibration and Flutter of Cylindrical and Conical Shells*, Air Force Office of Scientific Research, Air Research and Development Command, United States Air Force (1959).

[35] A. R. Staff, *Equations, Tables, and Charts for Compressible*

Flow, Tech. Rep. 1135, NASA Ames Aeronautical Laboratory, Moffett Field, California (1953).

[36] R. Pidaparti and H. T. Yang, Supersonic flutter analysis of composite plates and shells, *AIAA Journal,* 31 (6) (1993) 1109-1117.

[37] Y. C. Fung and M. D. Olson, Comparing theory and experiment for the supersonic flutter of circular cylindrical shells, *AIAA Journal*, 5 (10) (1967) 1849-1856.

Appendix

A. Conical shell linear equilibrium equations in terms of stress resultants

The principle parameters of conical shells can be obtained from the following equations:

$$A_1(x,\theta)=1, A_2(x,\theta)=x\sin(\alpha_c), \frac{1}{R_1(x,\theta)}=0, \frac{1}{R_2(x,\theta)} = \frac{1}{x\tan(\alpha_c)}, \frac{1}{\rho_{11}}=0, \frac{1}{\rho_{22}}=\frac{1}{x} \tag{A.1}$$

By introducing the geometrical parameters of conical shells into the general equilibrium equations of Sanders' improved linear theory [17], one obtains the equilibrium equations of a conical shell as follows:

$$\frac{\partial \mathrm{n}_{11}}{\partial x}+\frac{1}{x\sin(\alpha_c)}\frac{\partial \mathrm{n}_{12}}{\partial \theta}+\frac{1}{x}(\mathrm{n}_{11}-\mathrm{n}_{22}) -\frac{1}{2x^2\sin(\alpha_c)\tan(\alpha_c)}\frac{\partial \mathrm{m}_{12}}{\partial \theta}=0 \tag{A.2}$$

$$\frac{\partial \mathrm{n}_{12}}{\partial x}+\frac{1}{x\sin(\alpha_c)}\frac{\partial \mathrm{n}_{22}}{\partial \theta}+\frac{2\mathrm{n}_{12}}{x}+\frac{3}{2}\frac{1}{x\tan(\alpha_c)}\frac{\partial \mathrm{m}_{12}}{\partial x} +\frac{1}{x^2\sin(\alpha_c)\tan(\alpha_c)}\frac{\partial \mathrm{m}_{22}}{\partial \theta}+\frac{3}{2}\frac{1}{x^2\tan(\alpha_c)}\mathrm{m}_{12}=0 \tag{A.3}$$

$$\frac{\partial^2 \mathrm{m}_{11}}{\partial x^2}+\frac{2}{x^2\sin(\alpha_c)}\frac{\partial \mathrm{m}_{12}}{\partial \theta}+\frac{2}{x\sin(\alpha_c)}\frac{\partial^2 \mathrm{m}_{12}}{\partial x\partial \theta}+\frac{2}{x}\frac{\partial \mathrm{m}_{11}}{\partial x} -\frac{1}{x}\frac{\partial \mathrm{m}_{11}}{\partial x}+\frac{1}{x^2\sin(\alpha_c)^2}\frac{\partial^2 \mathrm{m}_{22}}{\partial \theta^2}-\frac{\mathrm{n}_{22}}{x\tan(\alpha_c)}=0 \tag{A.4}$$

Mehrdad Bakhtiari received his first master's degree in propulsion (KNTU-2009) and a second master's in industrial systems engineering (UofR-2014). He is currently a Ph.D. candidate in mechanical engineering at Polytechnique Montréal. His research interests are fluid structure interactions in thin shells.

Aouni. A. Lakis, is Full Professor at Department of Mechanical Engineering of Polytechnique de Montréal. He received his Ph.D. from McGill University. His research interest concerns are Aeroelasticity, dynamic stability, fluid-structure, numerical methods, plates and shells, Health monitoring.

Kerboua Youcef is research associate at Department of Mechanical Engineering of Polytechnique de Montréal. He did his Ph.D. under the supervision of Prof. Lakis. His research interest concerns are aeroelasticity, dynamic stability, fluid-structure, numerical methods, plates and shells.